CHAPTER 8

NONADIABATIC EXCITED-STATE DYNAMICS OF AROMATIC HETEROCYCLES: TOWARD THE TIME-RESOLVED SIMULATION OF NUCLEOBASES

MARIO BARBATTI*, BERNHARD SELLNER, ADÉLIA J. A. AQUINO, AND HANS LISCHKA*

Institute for Theoretical Chemistry, University of Vienna, Waehringerstrasse 17. A-1090, Vienna, Austria

Abstract: Ab inito molecular dynamics, although still challenge, is becoming an available tool for the investigation of the photodynamics of aromatic heterocyclic systems. Potential energy surfaces and dynamics simulations for three particular examples and different aspects of the excited and ground state dynamics are presented and discussed. Aminopyrimidine is investigated as a model for adenine. It shows ultrafast S_1-S_0 decay in about 400 fs. The inclusion of mass-restrictions to emulate the imidizole group increases the lifetime to about 950 fs, a value similar to the lifetime of adenine. The S_2-S_1 deactivation, typical in the fast component of the decay of nucleobases, is investigated in pyridone. In this case, the S_2-state lifetime is 52 fs. The hot ground-state dynamics of pyrrole starting at the puckered conical intersection is shown to produce ring-opened structures consistent with the experimental results

Keywords: Excited State, Heteroaromatic Molecules, Nonadiabatic Dynamics, Surface Hopping

8.1. INTRODUCTION

After UV photoexcitation the DNA and RNA bases return to the electronic ground state at an ultrafast time scale of about one picosecond [1]. Their short excited-state lifetimes imply an intrinsic stability against structural photoinduced changes. The characterization of the excited-state energy surfaces by means of stationary points, conical intersections and relaxation paths has been of fundamental importance for the understanding of the mechanisms taking place in the ultrafast deactivation of these bases [2–10]. In particular, theoretical investigations have shown the existence

* Corresponding authors, e-mails: mario.barbatti@univie.ac.at and hans.lischka@univie.ac.at

M. K. Shukla, J. Leszczynski (eds.), Radiation Induced Molecular Phenomena in Nucleic Acids, 209–235.

of several deactivation paths connecting the Franck-Condon region to conical intersections between the first singlet excited state and the ground state. These paths can be grouped into two types, those involving out-of-plane ring deformations and those involving planar bond-stretchings [7].

The full understanding of the complete ultrafast deactivation phenomenon involves time-dependent quantities, such as lifetimes and reaction rates, that call for the use of dynamics methods. Nevertheless, the dynamics simulation of nucleic acid bases and pairs is still a very challenging topic given the size and complexity of these molecular systems. The main limitation is the extremely high computational costs to obtain an appropriate description of the excited states, which requires quantum chemical multireference methods to provide a balanced description of the multitude of energy surfaces. Another important point is the dimensionality of the problem in terms of internal coordinates that should be taken into account. The fact that in heteroaromatic systems the conical intersections (and other important regions on the energy surfaces) involve strongly distorted structures precludes the restriction of the dynamics to few selected coordinates chosen by educated guesses. The usage of the full set of degrees of freedom seems to be mandatory eliminating, therefore, the systematic construction of potential energy grids in reduced dimensions. On the other hand, increasing computer power and improved quantum chemical methodology have made the direct or on-the-fly dynamics approach in classical dynamics calculations feasible even for high-level ab initio methods. In this approach all internal degrees of freedom are taken into account in an automatic way without any pre-computation of energy surfaces by calculating the electronic quantities (energies, energy gradients, etc.) as needed in the course of a trajectory.

For the simulation of nonadiabatic photochemical processes, the on-the-fly approach can be naturally implemented along with surface-hopping algorithms [11]. In photochemical processes usually sufficient initial energy is available from the vertical photoexcitation meaning that existing small energy barriers can be overcome and the region of the intersection seam can be approached in hundred of femtoseconds to few picoseconds. Because of the relatively short simulation times needed, such cases are specially tailored to an application of surface-hopping on-the-fly dynamics. The price to pay for using local approaches is that phenomena such as tunneling or vibrational quantization cannot be investigated.

The understanding of the energy surfaces is, of course, necessary for successful dynamics simulations. This knowledge is essential for selecting the appropriate quantum chemical method to be employed in the dynamics. Therefore, before presenting dynamics results we will discuss in some detail the features of the potential energy surfaces of heteroaromatic systems. The existence of conical intersections between the ground and the first excited states is to a large extent connected to the biradical character of the molecules in the excited state. For this reason, it is worth to discuss the relaxation paths and conical intersections of basic units such as ethylene and substituted ethylenes. We want to show that the understanding of these systems also helps to understand and classify the more complex situations of aromatic heterocycles. Finally, the dynamics of three distinct heterocycles will be presented, focusing in each case on a different aspect of the photochemical process.

8.2. METHODS IN AB INITIO ON-THE-FLY DYNAMICS

The description of molecules close to conical intersections normally is a multireference problem that demands the use of advanced methods for the treatment of the involved electronic states. The computational cost of on-the-fly ab initio dynamics is, as aforementioned, the main bottleneck for these simulations. If the time to compute one single point (excited state energy + gradient + nonadiabatic coupling vectors) is t_{sp}, the total cost of the dynamics is $n_{traj} \times n_{sp} \times t_{sp} \approx 10^6 t_{sp}$, where n_{traj} is the number of trajectories (typically $\leq 10^2$) and n_{sp} the number of single points in each trajectories (typically $\leq 10^4$). Although this situation is alleviated by the fact that the trajectories can run independently of each other, the ultrafast dynamics (few picoseconds) of a 6-membered heterocycle such as the pyrimidine bases is close to the limit of what can be treated considering the current computational capabilities.

Moreover, the method used to perform dynamics including all degrees of freedom should also allow the analytical computation of energy gradients and nonadiabatic coupling vectors. New semi-empirical methods have been worked out [12–16] within the framework of multiconfigurational wavefunctions. Semiempirical methods, however, have as major limitation the unpredictable quality of the potential energy surfaces in regions not spanned by the fitting of the parameters. Some methods such as the time-dependent density functional theory (TD-DFT) [17–19], the second-order coupled-cluster-based (RI-CC2) [20, 21] and the equation of motion-coupled cluster (EOM-CC) [22, 23] allow the computation of analytical gradients, but lack the multireference character. Others, such as density functional theory/multi-reference configuration interaction (DFT/MRCI) [24] or the family of multireference perturbation theory methods [25–28] can adequately describe the energies close to the conical intersections, but do not allow the computation of analytical gradients. It is worth noting that analytical gradients computed with complete active space second-order perturbation theory (CASPT2) have been recently developed [29] and this constitutes a promising fact for the near future.

Substantial progress has been made by the development of analytic energy gradients and nonadiabatic coupling vectors for multireference configuration interaction (MRCI) and state-averaged multiconfiguration self-consistent field (SA-MCSCF) approaches [30–34]. In particular, our group has worked on the development of methods and program systems for performing both, the quantum chemical and the dynamics calculations based on these methods. MRCI and SA-MCSCF calculations allowing the computation of analytical gradients and nonadiabatic coupling vectors [30, 32–34] can routinely be performed with the COLUMBUS program system [35, 36]. On-the-fly adiabatic and nonadiabatic (surface hopping) dynamics can be performed using these gradients and vectors with the NEWTON-X package [37, 38].

A full description of the outline and the capabilities of the NEWTON-X package is given elsewhere [38]. In brief, the nuclear motion is represented by classical trajectories computed by numerical integration of Newton's equations using the Velocity-Verlet algorithm [39]. Temperature influence can be added by means of the Andersen thermostat [40]. The molecule is considered to be in some specific

electronic state at any time and the nuclear trajectory is driven by the gradient of the potential energy surface of this state.

If the molecule is restricted to be in only one electronic state during the complete trajectory, the dynamics is termed adiabatic. On the other hand, imposing the electronic wavefunction to obey the time-dependent Schrödinger equation, the transition probability to jump from one potential surface to another can be obtained on the basis of either Tully's fewest switches algorithm [11, 41] or the modified fewest-switches algorithm proposed by Hammes-Schiffer and Tully [42]. In either case the decoherence correction developed by Granucci and Persico [43] can be applied. These algorithms statistically decide in which electronic state the system will stay in the next time step. When this option is activated, the dynamics is called nonadiabatic.

NEWTON-X has been developed in a highly modular way, with several independent programs communicating via files. At each integration time step of Newton's equations, NEWTON-X invokes a suitable external quantum chemical program and obtains the electronic energies, energy gradients, and nonadiabatic coupling vectors. In principle, any program that can supply analytical energy gradients and eventually analytical nonadiabatic couplings is eligible. For the time being, interfaces are provided for the quantum chemistry packages COLUMBUS [35, 36, 44], with which nonadiabatic and adiabatic dynamics using MCSCF and MRCI methods can be performed and TURBOMOLE [45] (adiabatic dynamics with CC2 or TD-DFT). Currently, an interface to the ACES II package [46] is under development.

As already discussed above, the adiabatic and nonadiabatic simulation of photochemical or photophysical processes requires the execution of a rather large number of trajectories. Each trajectory is completely independent of the others. Nevertheless, after having all trajectories completed, the data must be retrieved and stored together in such a way that all quantities of interest, such as quantum yields, state populations, and internal coordinates, can be computed as averages over all trajectories. NEWTON-X contains routines to generate ensembles of initial conditions for initiating several independent trajectories, to control the input and output of multiple trajectories, and to perform the required statistical procedures. In particular, in the examples discussed in this work the initial conditions for the simulated trajectories were generated by means of a ground-state quantum-harmonic-oscillator distribution of nuclear coordinates and momenta.

8.3. COMPUTATIONAL DETAILS

Throughout this work, several systems are discussed and the specific theoretical level is indicated in each case. The adopted notation is given as follows. CASSCF calculations including n electrons, m orbitals and averaging k states is denoted as SA-k-CASSCF(n, m). If all CAS configurations are used to build the reference space for the MRCI procedure, it is referred to simply as MRCI. On the other hand, if a different space with p electrons and q orbitals is used, it is denoted MRCI(p, q). The CI expansion includes either all single and double excitations (MR-CISD) or

only single excitations (MR-CIS) with respect to the configuration state functions describing the reference space. When single- and double-excitations are included, the generalized interacting space restriction [47] is adopted. Higher-order excitation effects are taken into account by means of the Davidson correction (+Q) [48–50]. The Pople basis sets 6–31G* and 6–31G are used [51, 52].

In the dynamics simulations, time steps of 0.5 fs were adopted for the integration of the Newton's equations. The time-dependent Schrödinger equation was integrated with the 5th-order Butcher algorithm [53]. The momentum after frustrated hoppings was kept constant and after actual hoppings it was readjusted along the nonadiabatic coupling vector.

Along this chapter, the structure of the conical intersections of several heterocycles will be discussed and described. Normally they correspond to different types of puckered rings and it is worth to use some systematic way to classify them. Among several possibilities (see [54] for a brief and recent review on this subject), we have adopted the Cremer-Pople approach (CP) [55, 56]. The Cremer-Pople approach is designed to give a mathematically well defined description of the shape of a puckered ring. It works by projecting the $3N$-6 internal coordinates of an N-membered ring onto a subspace of N-3 coordinates (or parameters). Each point in this subspace corresponds to a different conformation. Thus, two geometric structures differing by bond lengths or bond angles but still sharing the same N-3 coordinates are said to have the same conformation. The conformation can be further classified [57] (or alternatively decomposed [58]) in terms of the six canonical puckered rings, namely, chair (C), boat (B), envelope (E), screw-boat (S), half-chair (H), and twist-boat (T). To deal with conical intersections in heterocycles, we have adopted the conformer-classification and notation proposed by Boeyens [57] with the polar set of CP parameters (Q, θ, ϕ) [55]. While the Q parameter gives a general measurement of the puckering amplitude ($Q = 0$ Å corresponds to the planar ring), the θ and ϕ angles allow the continuous deformation from one conformation into another. For instance, the conformation $^1T_3$, corresponding to twist-boat shape with the atom 1 moved to above the ring-plane and the atom 3 moved to below, can be transformed either into the conformation $^4S_3$ (atom 4 above and atom 3 below the ring plane) by increasing θ or into $^{1,4}B$ (atoms 1 and 4 above the plane) by increasing ϕ. The advantage of adopting such a scheme will be evident when, for instance, in Section 8.5.1 we use these CP parameters to compare the minima on the crossing seam (MXSs) in aminopyrimidine and adenine. The calculations of the CP parameters were performed with the PLATON program [59].

8.4. EXCITED-STATE DEACTIVATION PATHS AND DYNAMICS OF SINGLE π-BONDS

The basic features of the relaxation paths and conical intersections in heteroaromatic rings can be understood in terms of the paths and intersections in ethylene and substituted ethylenes. As soon as a π electron is excited into the π^* orbital the

following two paths become energetically favorable. The first one is the well known twisting around the principal axis. The $\pi\pi^*$ state is stabilized and the S_0 state is destabilized. This leads to an avoided crossing between the S_0 and the S_1 states close to the 90° twisted structure. Bonačić-Koutecký et al. [60] have shown that the magnitude of the gap between S_1 and S_0 depends on the difference of the electronegativities between the two atoms of the double bond. For a non-polar system, the gap can be as large as 3 eV as it is in the case of ethylene, while it is very small for $CH_2NH_2^+$ (Figure 8-1a). Since the gap depends on the electronegativity, it can be modified by the application of external electromagnetic fields [61], by solvation effects [62], or – what is the most important case for the current discussion – by activation of other internal modes simultaneously to the torsion. In ethylene for instance this happens by activating the pyramidalization or hydrogen migration [63–65] modes (Figure 8-1c).

An important feature observed in torsional trajectories is that they often do not reach the crossing seam region at 90° even when the conical intersection exists there [66]. This happens because the gradient difference vector, one of the two vectors that linearly split the state degeneracy, points along the stretching coordinate of the main axis. Therefore, to reach the crossing seam after twisting demands a specific combination of torsional and stretching motions that gives the appropriate values of these coordinates at 90°. Normally this is not true and the actual value of the stretching corresponds to a finite gap (avoided crossing), in which the transition probability is relatively small. The consequence of the lack of correct phase between the torsion and the stretching is the increasing of the excited-state lifetime. Several torsional periods are required before the system decay, giving time to the activation of other internal modes. As a result, other regions of the crossing seam but the twisted configuration may be actually used to return to the ground state.

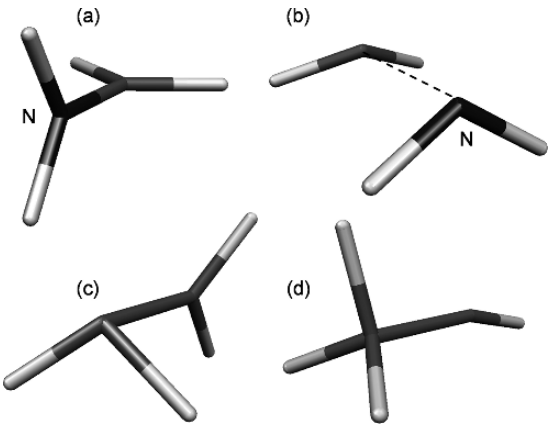

Figure 8-1. Conical intersections in ethylene (c and d) and $CH_2NH_2^+$ (a and b): (a) twisted, (b) stretched-bipyramidalized, (c) twisted-pyramidalized, and (d) ethylidene

The second type of relaxation process occurring for these polar π systems has been observed in both MRCI and CASSCF dynamics of $CH_2NH_2^+$ [38] and SiH_2CH_2 [66] systems and is characterized by a very strong stretching along the main axis with a simultaneous pyramidalization of both terminal groups (Figure 8-1b). This stretched-bipyramidalized conformation also gives rise to a S_0-S_1 conical intersection. Torsional and stretched-bipyramidalization types of trajectories are not completely separated and it is possible to observe trajectories with mixed features of both types.

The conical intersections at the stretched-bipyramidalized structures seem to be connected by the same crossing seam to the twisted conical intersection, as it has been observed in the case of $CH_2NH_2^+$ [38]. The large CN distances observed in this kind of conical intersection (2.24 Å at the minimum on the crossing seam, MXS) implies that specific dissociation channels could be activated after the decay to the ground state. In Section 8.5 we shall discuss the fact that while the twisted conical intersections are essential to understand the deactivation in heteroaromatic 6-membered rings [67], the stretched-bipyramidalized conical intersections seem to play an important role in heteroaromatic 5-membered rings [68].

It is worth mentioning that a third type of conical intersections appears in ethylene and substituted ethylenes after a hydrogen migration between two groups [63]. In ethylene, this process gives rise to the ethylidene isomer ($CHCH_3$, Figure 8-1d) [65, 69]. Although conical intersections were located for this kind of structure for ethylene and fluoroethylene [70], they do not constitute an important path to the decay [71]. Ethylidene-like conical intersections has been observed in the dynamics of substituted ethylenes mostly during the hot ground state motion after the decay, although some non-negligible fraction of trajectories in ethylene decays through it [71]. Moreover, these conical intersections may be important in the photodynamics of cyclohexene as well [69].

8.5. EXCITED-STATE DEACTIVATION PATHS IN HETEROCYCLES

It has been shown that a large variety of aromatic and heteroaromatic systems present conical intersections at specific out-of-plane distortions of one or more sites of the ring. For 5-membered rings they were found for pyrrole [68], imidazole, furan, thiophene, and cyclopentadiene [67]. Among the 6-membered rings for which these conical intersections were located we may mention benzene [72], cyclohexene [69], cyclohexadiene [73], stilbene [74], uracil [2], adenine [5–7], 2-aminopurine [9], pyrazine [72, 75], thymine [76], cytosine [77], pyridone [78], guanine [10], and aminopyrimidine [67]. In the case of 7- and 8-membered rings, conical intersections resulting from the out-of-plane distortion was already reported for azulene [79] and cyclooctatetraene [80]. In the following, we shall discuss in detail three specific examples, aminopyrimidine, pyridone and pyrrole, and see what the static

investigation of the excited state potential energy surfaces can tell about their photodynamics. Later in this chapter (Section 8.6), we will return to these examples within the context of dynamics simulations.

8.5.1. Case Study of 6-Membered Heterocycles I: Aminopyrimidine

Adenine and aminopyrimidine share strong structural similarities. For this reason the latter has been selected as a prototype for the study of the dynamics of purine bases [67]. Its first singlet excited state shows at least three different minima at SA-3-CASSCF(8,7)/6-31G* level of calculation, one of them being planar with $\pi\pi^*$ character. The two other minima of the S_1 state are slightly puckered at the C_2 and C_4 sites and have $n\pi^*$ character (for atomic numbering see Figure 8-2). Three distinct MXSs were found in aminopyrimidine. Their geometric structures are shown in Figure 8-2. The S_1-state energy and the Cremer-Pople parameters [55, 57] are given in Table 8-1.

All three MXSs can be reached with the excess energy of the vertical excitation. The ^2E and $^6S_1$ MXSs are completely analogous to MXSs identified in adenine [6, 7]. The $^4S_3$ MXS however does not occur in adenine due to the restrictions imposed by the imidazole group. The path connecting the C_2-puckered ($n\pi^*$) minimum of the S_1 state to the lowest-energy MXS (^2E) is shown in Figure 8-3a. Although a small barrier (0.19 eV) appears in this path, it should be noted that it is not the exact minimum energy path. It was obtained by linear interpolation of internal coordinates (LIIC) and, therefore, the barrier should be smaller or even inexistent. Figure 8-3a also shows the equivalent reaction path in adenine. The strong similarities between the paths for both systems are taken as an indication that they have

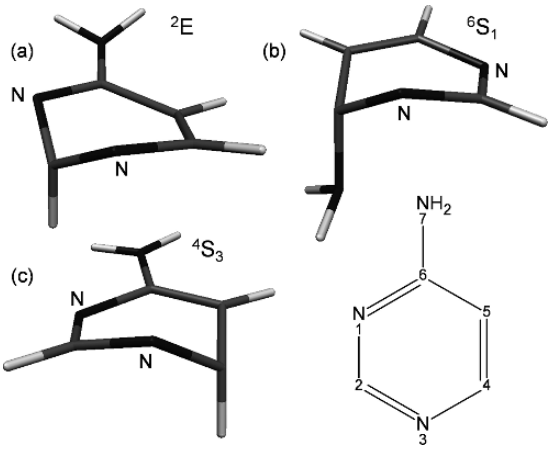

Figure 8-2. Minima of the crossing seam in aminopyrimidine: (a) ^2E, (b) $^6S_1$, and (c) $^4S_3$ (see Table 8-1). Calculations were performed at SA-3-CASSCF(8,7)/6-31G* level

Table 8-1. S_1 energy and Cremer-Pople parameters for the ring puckering conical intersections in aminopyrimidine, pyridone and pyrrole. Energies relative to the S_0 energy in the ground state equilibrium geometry. The values in parenthesis are the CP parameters for the equivalent MXSs in 9H-adenine using the geometries given in [5]

MXS	ΔE (eV)	Q (Å)	θ(°)	ϕ(°)	Conformation
Aminopyrimidine[a]					
Figure 8-2a	4.49	0.54 (0.52)	111 (114)	250 (246)	envelope ^2E
Figure 8-2b	4.60	0.50 (0.48)	119 (120)	147 (153)	screw-boat $^6S_1$
Figure 8-2c	4.79	0.53	118	333	screw-boat $^4S_3$
Pyridone[b]					
Figure 8-4a	4.31	0.34	84	314	boat $B_{3,6}$
Figure 8-4d	4.45	0.55	113	142	screw-boat $^6S_1$
Figure 8-4c	4.80	0.13	61	78	screw-boat $^3S_2$
Figure 8-4b	5.51	0.62	61	183	envelope E_4
Pyrrole[c]					
Figure 8-5a	5.52	0.43	–	1	envelope E_1

[a] SA-3-CASSCF(8,7)/6-31G*; [b] SA-3-CASSCF(10,8)/6-31G; [c] SA-2-CASSCF(6,6)/6-31G*.

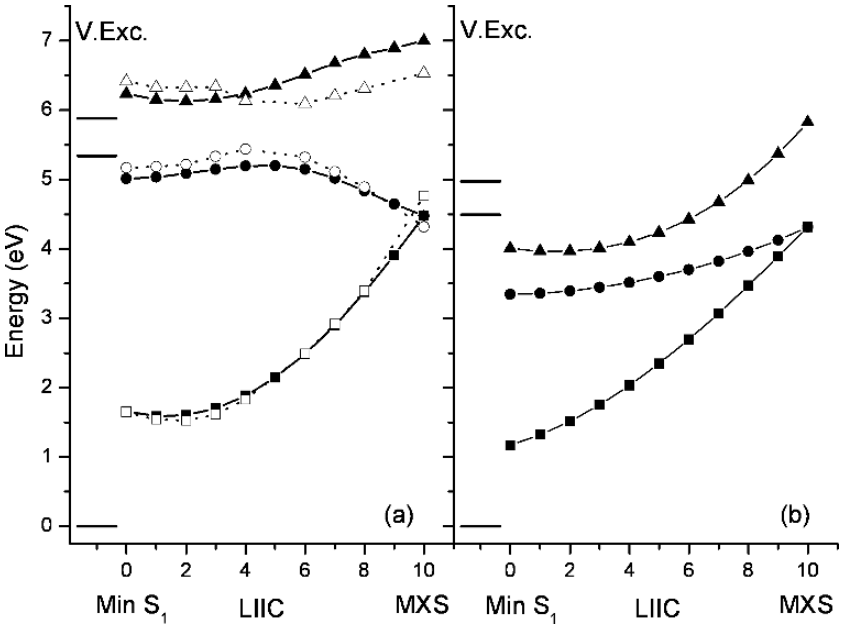

Figure 8-3. LIIC between the minimum of the S_1 state and the S_1/S_0 MXS in (a) aminopyrimidine and (b) pyridone. Calculations performed at (a) SA-3-CASSCF(8,7)/6-31G* and (b) SA-3-CASSCF(10,8)/6-31G levels. Open symbols in (a) show the equivalent curves in 9H-adenine according to [7]. The S_1 and S_2 vertical excitation energies are indicated at the left side of each graph

similar behavior after photoexcitation. Nevertheless, the dynamics simulations will show that different processes are taking place in the two cases.

All this information about the S_1 and S_0 states suggests that aminopyrimidine will present ultrafast decay through puckered conical intersections. The excited-state lifetime and the actual conical intersection that participate in the deactivation process can only be found by dynamics simulations (see below).

8.5.2. Case Study of 6-Membered Heterocycles II: Pyridone

Pyridone is a fluorescent analogue of the pyrimidine bases that has been used in Watson-Crick-pair models [78, 81, 82]. One minimum on the S_1 surface has been found in pyridone. At the SA-3-CASSCF(10,8)/6-31G level, it has a planar structure and $n_O\pi^*$ biradical character. Frey et al. [78] found a MXS in pyridone ($^6S_1$, see Table 8-1). In addition to this we located other three MXSs as well (Figure 8-4). The MXSs with the lowest energies are the $B_{3,6}$ (Figure 8-4a) and the $^6S_1$ (Figure 8-4d). The MXS with the highest energy corresponds to a simple envelope puckering (E_4) (Figure 8-4b). The last MXS ($^3S_2$), with intermediary energy, is only slightly puckered as can be observed from the puckering amplitude Q = 0.13 Å in Table 8-1. One of its main features is the sp^3 hybridization (pyramidalization) of the C_2 site.

The vertical excitation into the $\pi\pi^*$ state (S_2) amounts to 4.97 eV. Therefore, from an energetic point of view two MXSs are available with the existing energy excess. Since the S_1 and S_2 states are quite close it can be supposed that in the

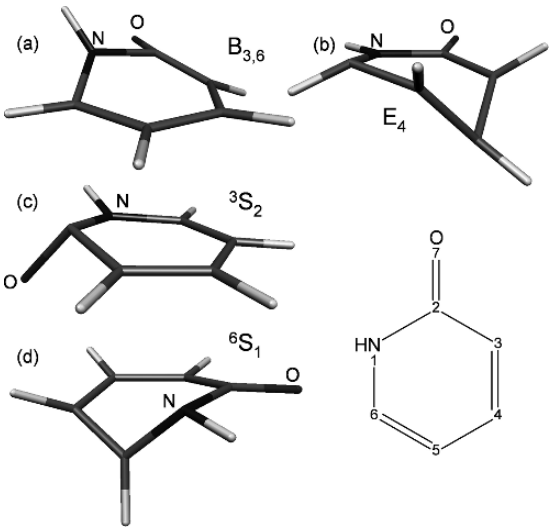

Figure 8-4. Minima of the crossing seam in pyridone: (a) $B_{3,6}$, (b) E_4, (c) $^3S_2$, and (d) $^6S_1$ (see Table 8-1). Calculations were performed at SA-3-CASSCF(10,8)/6-31G level

first stage of the relaxation process pyridone quickly decays to S_1. The relaxation will lead to the minimum on the S_1 surface. From there, pyridone could reach the conical intersection region by an up-hill path as shown by the LIIC path connecting the minimum of the S_1 state to the MXS of lowest energy ($B_{3,6}$) in Figure 8-3b. Although it has enough energy, pyridone does not seem to follow this path, as it is revealed by the fact that it is a fluorescent species. It is worth noting that this situation is probably not a consequence of the theoretical method used. MR-CISD+Q(6,5)/SA-3-CAS(10,8)/6-31G calculations [83] also show the vertical S_1 and S_2 excitations higher than the lowest MXS.

8.5.3. Case Study of 5-Membered Heterocycles: Pyrrole

Out-of-plane distortions play an important role to reach conical intersections in 5-membered rings as well [68]. In these cases, however, the out-of-plane distortion is accompanied by ring opening at the puckered site (see Figure 8-5a and Table 8-1). In this section it is discussed in some detail the occurrence of this type of conical intersection, the paths to reach it, and other competing deactivation paths in pyrrole. Later, in Section 8.5.4 the generality of these features will be considered as well.

Despite the fact that pyrrole cannot be considered as a direct model for nucleic acid bases, it is particularly interesting because it contains two completely different reaction paths also present in 9H-adenine, namely the out-of-plane deformation and the H-detachment [7, 8]. In pyrrole, these two paths are energetically available after $\pi\pi^*$ excitation. Therefore, the question concerning their relative importance for the photodynamics needs to be answered.

The first deactivation path identified in pyrrole was the H-detachment (Figure 8-6 *left*), which promotes the crossing between the S_0 and the S_1 ($\pi\sigma^*$) states (Figure 8-5b) [84]. Although the deactivation through this conical intersection can

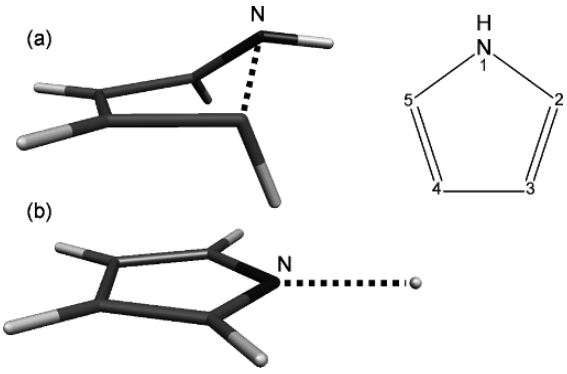

Figure 8-5. Minima of the crossing seam in pyrrole. Calculations were performed at (a) MR-CISD/SA-3-CASSCF(6,5)/6-31G* and (b) MR-CISD/SA-3-CASSCF(6,6)/6-31G* levels. Dashed lines indicate (a) the ring opening (E_1) and (b) the H-detachment

explain the existence of hydrogen atoms among the photofragments, it cannot explain the origin of HCN and CNH_2 that follows the photofragmentation [68, 85]. Recently, we showed the existence [68] of a ring opening out-of-plane deformation (Figure 8-6 *right*) that generate a conical intersection in pyrrole. We have also argued that the path to this conical intersection is a main photochemical path that could explain the occurrence of these other fragments and even part of the hydrogen-atom elimination. These conclusions were based on the analysis of reaction paths on the potential energy surfaces. Specific points such as how much and when each path is populated require dynamics simulations. An important factor determining the complexity in the photodynamics of pyrrole is that besides the ground and two $\pi\pi^*$ states, at least two Rydberg ($\pi - 3s(\sigma^*)$) states will be involved in the deactivation process (see Figure 8-6 *right*). These five states form an intricate sequence of conical intersections. Along the H-detachment path, the $\pi\pi^*$ states are destabilized while the Rydberg states are stabilized until they intersect with the ground state. On the other hand, along the ring-opening deactivation path, the Rydberg states and one $\pi\pi^*$ state are destabilized while the other $\pi\pi^*$ state is stabilized and intersects the ground state.

In the present work dynamics of pyrrole in the excited state will not be discussed. Instead, in Section 8.6 we will present dynamics simulations for the investigation

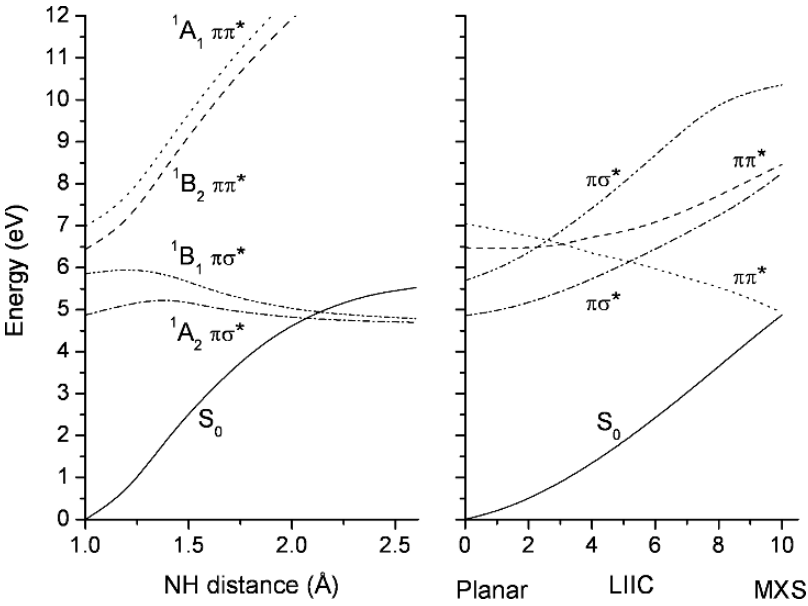

Figure 8-6. H-detachment (*left*) and ring-opening (*right*) deactivation paths in pyrrole. Both paths start at the ground state equilibrium geometry. Calculations at MR-CISD level (see [68] for details on the calculations)

of the reactivity of pyrrole in the hot ground state, which is generated by the decay at the ring-opening conical intersection.

8.5.4. General Discussion on the Deactivation Paths in Heterocycles

The simplest out-of-plane distortion in a 6-membered ring that results in a conical intersection is the puckering at one site. This process strongly destabilizes the ground state, but has the opposite effect in a biradically excited state because it decouples the biradical centers. For instance, for a $\pi\pi^*$ state, the puckering leads to a singly-occupied π orbitals almost perpendicular to the π^* orbital, exactly as it occurs in the case of twisted MXSs in substituted ethylenes discussed above (see Figure 8-7b) [86]. One way to understand this relaxation process is to look at the puckering as a result from the torsional motion around specific bonds (Figure 8-7a) [67] analogous to the torsion in simple biradical models. The geometrical constraints are now strong and the "torsional" motions appear as a puckering of one site of the ring (envelope conformation).

The envelope conformation is, however, only a particular case of out-of-plane distortions that are able to generate conical intersections in aromatic and heteroaromatic rings. We have already seen in the previous sections examples of conical intersections with screw-boat and boat conformations arising in aminopyrimidine and pyridone. In all these cases, the relaxation on the excited-state surface is

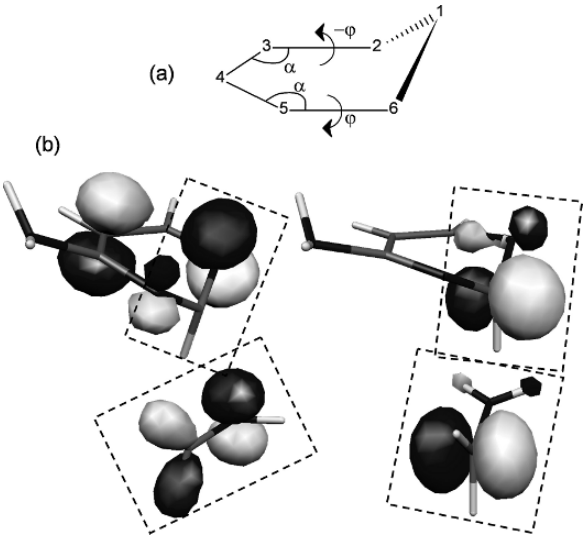

Figure 8-7. (a) Puckering around one site in a six-membered ring. The drawing should be seen as a general prototype for heteroaromatic systems, containing one or more heteroatoms. (b) Singly-occupied orbitals in the S_1 state of aminopyrimidine at the ^{2}E MXS geometry (*top*). The important sites for the comparison with $CH_2NH_2^+$ orbitals at the twisted MXS geometry (*bottom*) are indicated by the dashed rectangles

regarded the same as before: the torsion of bonds promoting the decoupling of biradical centers.

The distinction between the deformations in 6- and 5-membered rings is connected to their respective constraints. Consider for instance a 6-membered ring. The puckering of one specific site, say site 1 in Figure 8-7a, is generated by twisting the dihedral angles φ (4561 and 4321). In order to make this conjugated twisting possible keeping the same bond lengths, it is necessary at same time to reduce the angles α (456 and 432) to values smaller than the original 120°. The reason for puckering at site 1 is to have a *p*-like orbital at this site orthogonally oriented in relation to the π-system (biradical decoupling relaxation). This situation, however, implies a very strong reduction of the α angles (by about 20°), leading to a significant strain in the sp^2 bonds. MXS optimizations for several 6-membered rings [7, 67] have shown that normally the *p*-like orbital is twisted by only 60°–70° in relation to the π system (measured by the 5612 dihedral angle, for example), corresponding to a smaller reduction of the α angles (about 10°) and consequently to less strain in the sp^2 bonds. From this configuration, which is geometrically similar to the twisted MXS in substituted ethylenes, the relaxation of the bond lengths and additional bond angles is able to tune the conical intersection. Note that in order to keep the sp^2 hybridization, the non-ring atoms or groups attached to sites 2 and 6 should also move out of the ring plane.

The reduction of the α angles during the puckering has the effect of shortening the distance between the sites 2 and 6 creating, as pointed out by Bernardi et al. [87], a partial σ-bond connecting these sites. As a result, the puckering gives rise to the bycyclic structures such as the prefulvene conical intersection typical of the benzene photodynamics [88]. For 5-membered rings the symmetrical puckering of site 1 by 65°, similar as in 6-membered rings, requires that the valence angles (543 and 432) are reduced by about 15°. An energetically less expensive alternative is to twist only one bond, say φ (4321 in Figure 8-8a). The consequence is the breaking of a bond and the opening of the ring. As before, in order to keep the hybridization scheme requires the motion of the atoms attached to site 2 out of the ring plane. The resulting configuration is geometrically similar to the stretched-bipyramidalized conical intersections in substituted ethylenes. Besides pyrrole, this type of conical intersections have been also identified in imidazole, furan, thiophene, and cyclopentadiene [67]. Out-of-plane ring-opening processes in 5-membered rings are also responsible for the photoisomerization of dihydroazulene into vinylhepafulvene [89].

The main difference between these stretched-bipyramidalized conical intersections in rings and substituted ethylenes is the process by which they are reached. As already discussed before (Section 8.4), dynamics calculations [38, 66, 90] showed that an important fraction of trajectories of polar substituted ethylenes undergoes stretching and bipyramidalization in the beginning of the time evolution. Nevertheless, in rings the "stretched-bipyramidalized" configuration cannot be reached by the direct activation of these modes, but it is obtained indirectly as a consequence of the torsional motion around specific bonds. Despite the fact

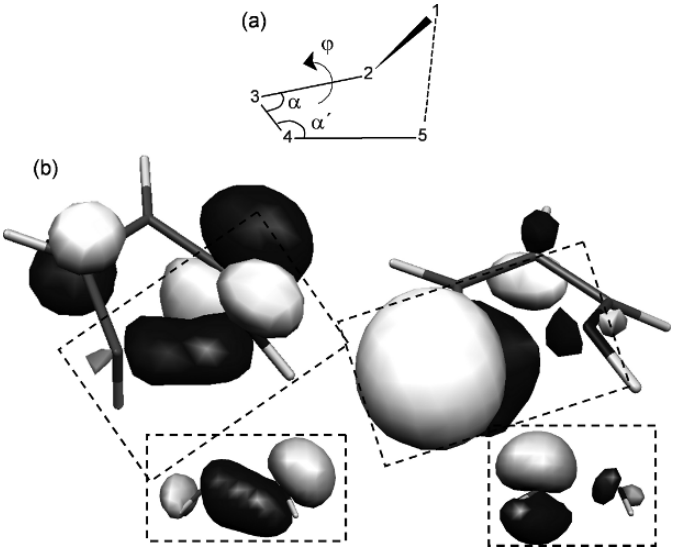

Figure 8-8. (a) Puckering around one site in a five-membered ring. The drawing should be seen as a general prototype for heteroaromatic systems, containing one or more heteroatoms. (b) Singly-occupied orbitals in the S_1 state of pyrrole at the MXS geometry (*top*). The important sites for the comparison with $CH_2NH_2^+$ orbitals at the stretched-bipyramidalized MXS geometry (*bottom*) are demarked by the dashed rectangles

that rings and substituted ethylenes reach the stretched-bipyramidalized region of the crossing seam in distinct ways, their electronic structures keep strong resemblance. For instance, Figure 8-8b shows the two singly-occupied orbitals in the ring-opening MXS of pyrrole and also the two singly-occupied orbitals in the stretched-bipyramidalized conical intersection of $CH_2NH_2^+$. The same geometric and electronic features can be observed in both cases, including the strong $\pi - \sigma$ mixing in the orbitals at the left side of the figure.

Recently, Perun et al. [8] investigating the imidazole group in adenine and Salzmann et al. [91] analyzing thiophene observed that the opening of these 5-membered rings under planarity restriction produces a S_0/S_1 conical intersection of $\pi\sigma^*$ character. The just mentioned $\pi\sigma$-mixing observed in the ring-opened out-of-plane conical intersection (Figure 8-8b) is an indication that the planar structures should be considered as a special case of the structures that have been discussed here. It is quite likely that the crossing seam connects the planar and the out-of-plane structures. This is also a possibility in the case of azulene, for which planar [89] and non-planar [79] conical intersections involving the same sites have been identified.

Conical intersections with ring opening configurations do not occur only in 5-membered rings. In the case of cyclohexadiene [73] and related systems, such as chromenes [92] and pre-vitamin D [93], the puckering process can be rationalized

as the torsion around two bonds, 2-3 and 4-5 in Figure 8-7a, opening the ring at bond 1-6. The conical intersection obtained in this way does not correspond to the minimum on the crossing seam [73]. The MXS occurs for an asymmetric configuration with the torsion occurring mostly at one bond. Also in this case, the system ends up at a ring-opened structure. In the case of cyclohexadiene, Garavelli et al. [73] have shown that these conical intersections are connected by the same crossing seam.

We have seen that in pyridone the $^3S_2$ MXS has a very small degree of puckering. This was observed in cyclohexene too [69], for which the conical intersection can be formed by slight out-of-plane deformation of the ring, compensated by strong readjustment of the hydrogen atoms. In cyclohexene, this produces a geometric configuration similar to pyramidalized ethylene [65]. It is expected that this kind of conical intersection may be particularly common in rings containing only one double bond or when groups or atoms with π and lone pairs are attached to the ring.

8.6. NONADIABATIC EXCITED STATE DYNAMICS OF HETEROCYCLES

Figure 8-9 shows basic schemes on how heterocyclic systems can reach conical intersections based on ring puckering modes. After photoexcitation the ring undergoes an initial, basically in-plane relaxation, which brings it to the S_1 minimum. Depending on the barrier height the molecule can simply stay trapped there until it decays via photo-emission. In the situation that seems to be typical for nucleobases, the barrier height is small enough so that the system may stay in this minimum for a period of time that ranges from hundreds of femtoseconds to few picoseconds, but it finally overcomes the barrier. Thereafter, the second phase of the relaxation process starts and it finishes at a conical intersection through which the system returns to the ground state. After that, the initial compound can be restored or different reaction products can be obtained. The complexity of this scenario would be further increased by taking into account that the photoexcitation does not

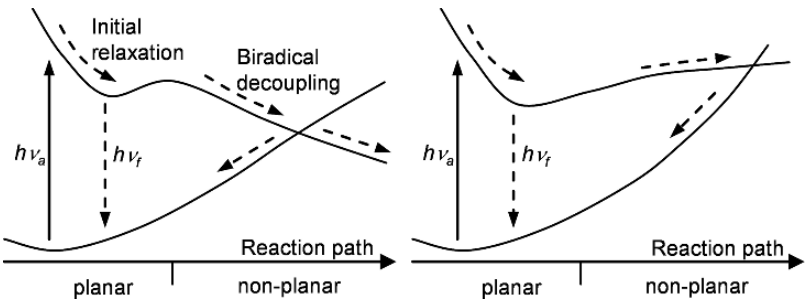

Figure 8-9. Two schematic reaction paths connecting the Franck-Condon region with the conical intersection

always lead to the first excited state, which means that the system has to find its path down through a set of consecutive conical intersections involving different excited states. In the discussion that follows, all these points will be highlighted by looking at: (i) the relaxation in the first excited state and the deactivation to the ground state of aminopyrimidine, (ii) the initial decay involving multiple excited states in pyridone, and (iii) the processes occurring in pyrrole in the hot ground state after the radiationless decay has taken place.

8.6.1. The S_1-S_0 Deactivation: Aminopyrimidine

Bicyclic rings such as the purine bases are still at the edge of current computational capabilities for performing multireference ab initio excited state dynamics. Therefore, we decided to investigate the ultrafast deactivation of adenine using a simplified model. Although two of the identified deactivation paths in 9H-adenine involve deformations at the imidazole ring, the most probable deactivation path dominating in low excitation energies is expected to be the puckering of the pyrimidine ring at the C_2 site (see numbering in Figure 8-2) [5–8]. The central role of the C_2 site can be deduced from the very long lifetime of 2-aminopurine [1], indicating that the new position of the amino group inhibits the deformation at the C_2 site. Hence, if the imidazole ring can really be neglected during this kind of photodynamics, aminopyrimidine seems to be a natural candidate to a model for adenine. It is also encouraging to observe that, as discussed in Section 8.5.1, there are strong similarities between the relaxation paths and MXS structures of aminopyrimidine and adenine.

Excited state nonadiabatic dynamics for thirty trajectories of aminopyrimidine were performed using a maximum simulation period of 800 fs [67]. Our primary goal was the characterization of the actually occurring low-energy deactivation path from the several available (Section 8.5.1). After starting the trajectories in the S_1 ($^1\pi\pi^*$) state, aminopyrimidine quickly returns to the ground state with a lifetime of 416 ± 150 fs. The potential energies of S_0 and S_1 states are shown in Figure 8-10 (*top*) for a typical trajectory. The main reaction path driving aminoyprimidine to the intersection involves the puckering at the C_4H group, corresponding to the $^4S_3$ MXS depicted in Figure 8-2c. Even though about 75% of the trajectories that decay have followed this path, the remaining 25% follow the out-of-plane deformation involving mainly the N_3 atom. None of the trajectories deactivated via conical intersections with NH_2 out-of-plane bending shown in Figure 8-2b.

The predominance of the nonadiabatic deactivation involving puckering at the C_4 atom is not favorable for using aminopyrimidine as a model for adenine. In adenine the imidazole group is connected to the atoms C_4 and C_5 of pyrimidine, which cannot be expected to allow any strong out-of-plane deformation due to structural restrictions. In order to introduce these restrictions in a simple way into aminopyrimidine, the structural effect of the imidazole ring was simulated by assigning heavier masses to the hydrogen atoms connected to C_4 and C_5. The isotopic mass of these hydrogen atoms was chosen to be 45 a.m.u, which produces

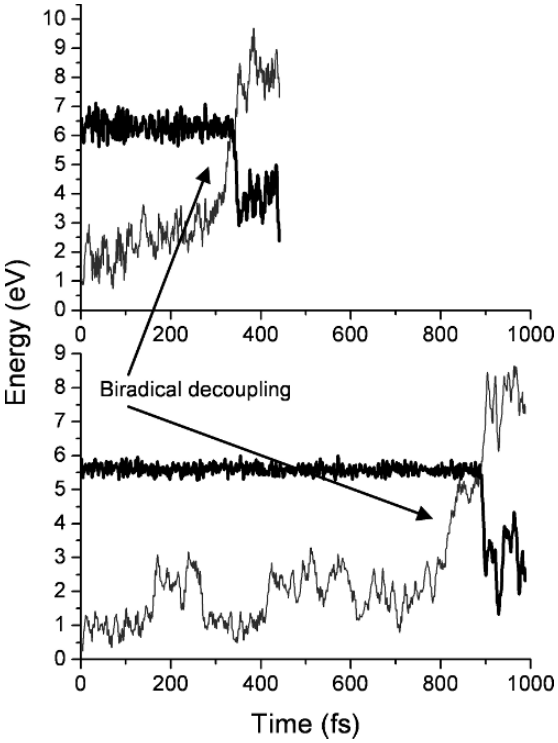

Figure 8-10. S_0 and S_1 potential energies versus time for two typical trajectories of normal (*top*) and mass-restricted (*bottom*) aminopyrimidine. The thick line indicates the current state. Simulations performed at SA-2-CASSCF(8,7)/6-31G* level

a moment of inertia for the out-of-plane motion that equals the moment of inertia of the center-of-mass of the imidazole group. Subsequently, a new set of 30 trajectories was computed for a simulation period of 1700 fs.

The mass-restriction has a significant effect on the dynamics simulations. The lifetime increases to 957 ± 200 fs, which is a value notably similar to the experimental lifetime of adenine (1.0 ps [1]). The potential energies of S_0 and S_1 states for a typical trajectory are shown in Figure 8-10 (*bottom*). The puckering at the C_4H group was to some extent inhibited and the main path to the crossing seam is the out-of-plane deformation involving the N_3 atom and, in some cases, the C_2 atom as well.

In both the mass unrestricted and restricted cases, the analysis of individual trajectories showed that the dynamics passed through three phases. First, a very fast relaxation process occurred leading to the minimum on S_1 surface. This step took not more than 100 fs independently of the isotopic masses. The character of the state changed from $\pi\pi^*$ to $n\pi^*$. In the second step, aminopyrimidine oscillates around the S_1 minimum keeping the $n\pi^*$ character. This step is strongly dependent

on the isotopic mass. In normal aminopyrimidine the path to the puckering was found in about 300 fs, while in the mass-restricted aminopyrimidine it took about 800 fs. Finally, in the third step the S_1 state changed its character to $\pi\pi^*$ and S_1 stabilized until finding the crossing seam. This is again a fast step that takes not more than 100 fs and does not depend on the mass-restriction. The description of the photodynamics of aminopyrimidine could be compared with the general process illustrated in Figure 8-9 (*left*). The first step corresponds to what was called initial relaxation in that figure, while the third step (see Figure 8-10) is the biradical decoupling.

Further investigations on the dynamics starting in the S_2 state are reported elsewhere [94].

8.6.2. The S_2-S_1 Deactivation: Pyridone

It has been observed (see Figure 8-3) that even though the $\pi\pi^*$ excitation energy is large enough to reach different regions of the crossing seam, pyridone is a fluorescent species and the nonadiabatic decay is not the main mechanism for the deactivation. The main reason for this behavior could be connected to the evidence that the crossing seam region cannot be reached by a sequence of excited-state relaxations, as in aminopyrimidine, because it is too high in comparison to the S_1 minimum.

In the present work the discussion is concentrated on the deactivation from the S_2 to S_1 state, which occurs in less than 200 fs. This topic is particularly relevant for the photodynamics of adenine [95], whose bright $\pi\pi^*$ state is not the S_1 state and the relaxation on the excited state surfaces should occur through a sequence of conical intersections. Indeed, Canuel et al. [1] have experimentally observed that the ultrafast decay of the nucleobases follows a biexponential pattern, whose fast component has a life time in the range of 100 (adenine) to 148 fs (guanine). The fact that pyridone does not return radiationlessly to the ground state simplifies the investigation of this first stage of the dynamics, reducing the decay to a monoexponential pattern.

The dynamics simulation was performed including three states, S_0, S_1 and S_2. Thirty-five trajectories were run for 200 fs with time step 0.5 fs. The ab initio calculations were performed at SA-3-CASSCF(10,8)/6-31G level. The numbering scheme is shown in Figure 8-4.

The first step in the dynamics, the S_2-S_1 deactivation, is completed in only 52 $\pm$ 1 fs, presenting the expected monoexponential decay profile, as can be seen in Figure 8-11a. This figure shows the fraction of trajectories in each state between 0 and 200 fs for the 35 trajectories computed. Between 20 and 30 fs and again at 37 fs it is possible to observe a revival of the S_2 state occupation. The fraction of trajectories in S_1 is not shown in the figure for sake of clarity. It is just complementary to the fraction of trajectories in S_2. Thus, a revival in S_2 is companied by a decrease in S_1 occupation. The revivals in the S_2 occupation occur when the total number of

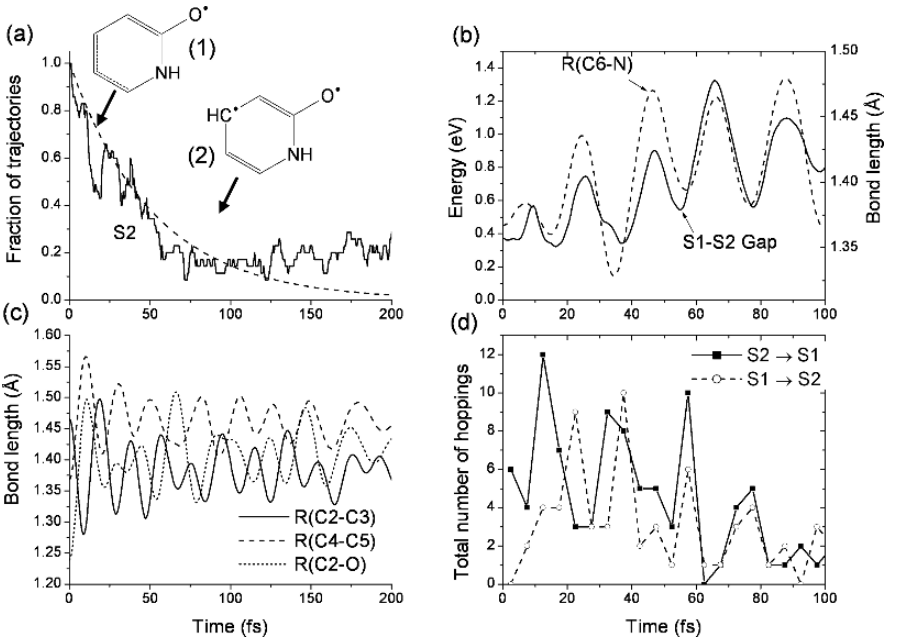

Figure 8-11. Initial photodynamics of pyridone: (a) Fraction of trajectories in each adiabatic state. The exponential decay curve was obtained by fitting of the S_2-state occupation, (b) averaged S_1-S_2 energy gap and averaged C_6N bond length, (c) averaged C_2C_3, C_4C_5, and C_2O bond lengths, (d) Total number of hoppings (S_2–S_1) and back-hoppings (S_1–S_2). All quantities in function of time. Calculations performed at the SA-3-CASSCF(10,8)/6-31G level

S_2-S_1 hoppings at a certain time is smaller than the total number of S_1-S_2 hoppings (Figure 8-11d).

For each trajectory the S_2-S_1 decay is not composed by a single hopping event, but by a series of forth and back hoppings. The hopping probability is enhanced by relatively small S_1–S_2 energy gaps (compare Figure 8-11b and d). The gap value on its turn depends on the in-plane vibrations of the pyridone ring. In particular, in the first 100 fs the averaged S_1–S_2 energy gap is correlated to the C_6N bond length and the minimum energy gap occurs at every time that this distance also reaches its minimum (Figure 8-11b). In this situation the π_N orbital delocalizes over the C_6 and C_2 atoms and stabilizes the $\pi\pi^*$ state.

This initial 200 fs dynamics is dominated by the planar relaxation of pyridone. The CO bond average length increases from 1.24 Å to 1.50 Å in only 10 fs and after that it oscillates around 1.41 Å (Figure 8-11c). It means that the oxygen atom becomes a radical center (see structure (1) in Figure 8-11a). After 50 fs, when the system is already in the S_1 ($n\pi^*$) state, the bonds in the ring are reorganized in such a way that a second radical center emerges at the C_4 atom. This biradical

conformation (structure (2) in Figure 8-11a) describes also the conformation that the minimum on the S_1 surface assumes.

In general, the S_2–S_1 deactivation can take place in two distinct ways depending on whether the character of the electronic state is preserved or not. In the case of pyridone the analysis of the trajectories shows that the character is changed from $\pi\pi^*$ to $n_O\pi^*$ when the decay to S_1 occurs. Frey and co-workers [78] have experimentally shown that the photoexcitation of out-of-plane vibrational modes of the S_1 state can drive pyridone towards a conical intersection, thus quenching the fluorescence emission, while in-plane modes do not produce the same effect. This is an interesting observation that sheds light on the actual importance of the out-of-plane deformations to the photodynamics of heterocycles. This process, however, should take place at the picosecond time-scale. Corresponding calculation results can be found in reference [83].

8.6.3. Dynamics After Internal Conversion: Pyrrole

The experimental data about pyrrole photofragmentation show that a large amount of HCN is formed. This amount corresponds to about half of the fragments when the photo-excitation is performed into the $^1B_2\pi\pi^*$ state [85]. Based on the analysis of the potential energy surfaces (see Section 8.5.3), we have shown the existence of a ring-opening process that could account for these fragments [68].

The first question that dynamics should be able to address is how the excited state population is distributed between the two deactivation paths (N-H dissociation and ring puckering). Nevertheless, excited-state dynamics simulations of pyrrole is particularly challenging because, as we have discussed in Section 8.5.3, the Rydberg states cannot be neglected and a total of four excited states must be included. In this section the aspects of the post-deactivation dynamics that depend essentially on the ground state surface are discussed. If the out-of-plane ring-opening MXS is responsible for HCN fragments, it is expected that the radiationless decay to the ground state through the ring-opening conical intersection (Figure 8-5a) should give rise to non-cyclic species and not only return to the initial pyrrole geometry.

In order to investigate the available reaction channels and in particular the feasibility of the ring opening process, the dynamics calculations were started on the ground state surface at the geometry of the ring-opening MXS (Figure 8-5a). It is expected that after decaying through a conical intersection the system preferentially follows the two directions that define the cone [96, 97]. For this reason we have scanned the plane defined by these directions, namely the gradient difference vector $2\mathbf{g} = (\nabla_R E_1 - \nabla_R E_0)$ and the nonadiabatic coupling vector $\mathbf{h} = \langle \Psi_1 | \nabla_R \Psi_0 \rangle$. In these equations, E_k and Ψ_k, $k = 0, 1$, are the adiabatic energies and the electronic wave function of state k. The sub-index R in the differential operator indicates that that the derivative is performed with respect to the nuclear coordinates. An arbitrary direction in the $(\mathbf{g}, \mathbf{h})$ plane is written in terms of a linear combination of their unit vectors as $\hat{\varepsilon} = \left(\hat{\mathbf{g}} \sin\alpha + \hat{\mathbf{h}} \cos\alpha\right)$. The initial velocity $\mathbf{v}_0$ is defined along $\hat{\varepsilon}$ with

its modulus corresponding to a predefined kinetic energy ΔE:

$$\mathbf{v}_0 = \left(\frac{2\Delta E}{\sum_i M_i \varepsilon_i^2} \right)^{1/2} \hat{\varepsilon}, \tag{8-1}$$

where M_i is the mass of atom i and ε_i, the component-vector of $\hat{\varepsilon}$ at atom i. The initial kinetic energy should be smaller than the maximum energy available $\Delta E_{\max} = E_{Vexc} - E_{MXS} = 1.89\text{eV}$ (at MR-CISD/SA-3-CASSCF(6,5)/6-31G* level) and lager than the kinetic energy defined by simple equipartition among all internal degrees: $\Delta E_{\min} = 2\Delta E_{\max}/(3N-6) = 0.16\text{eV}$. In these equations E_{Vexc}, E_{MXS}, and N are the vertical excitation energy, the potential energy at the MXS geometry and the number of atoms, respectively. The factor 2 comes from the fact that two degrees of freedom are needed to define the (**g**-**h**) plane.

Following this prescription, we have performed dynamics simulations with initial velocities pointing along 24 different directions in the **g**-**h** plane and with several initial kinetic-energy values between the maximum and the minimum. The results are presented in Figure 8-12. This figure shows the CN distance in pyrrole after 40 fs (radial coordinate) as a function of the initial direction (angular coordinate). Most of initial directions lead to a CN distance of around 1.5 Å and do not result in non-cyclic structures. In these cases they correspond to photophysical

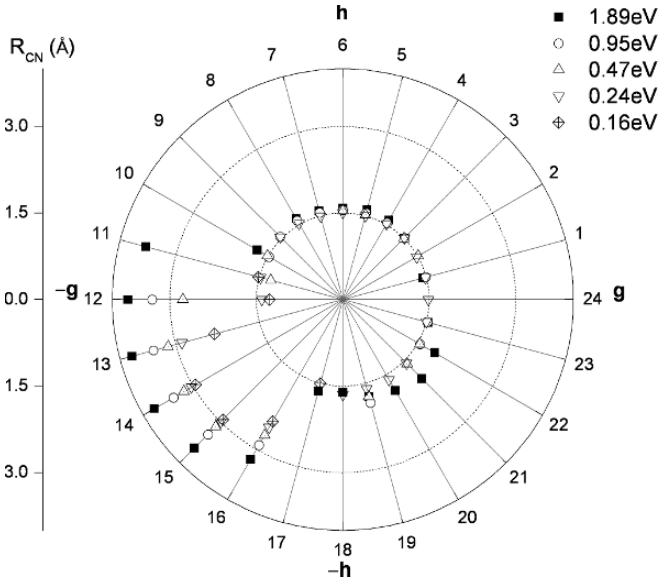

Figure 8-12. CN distance (radial coordinate) after 40 fs in pyrrole ground-state dynamics starting at the ring-opening MXS, in function of the initial velocity direction (angular coordinate) in the (**g**–**h**) branching space. Calculations performed at the SA-2-CASSCF(6,6)/6-31G* level

processes that are expected to end up in a hot pyrrole ground state. There is however a special subset of directions between –**g** and –**h** whose CN distance is about 3 Å, showing the formation of non-cyclic species. They correspond to photochemical processes consistent with the HCN elimination experimentally observed [85]. A similar analysis at 80 fs shows that the CN distances is still about 1.5 Å for the first type of trajectories, while the CN distance increased to about 4.5 Å in the trajectories with non-cyclic structures. The number of trajectories that result in non-cyclic structures depends not only on the initial velocity direction but also on the initial kinetic energy (see Figure 8-12). Thus, while with $\Delta E = 0.16$ eV only directions between 13 and 16 are photochemical channels, with $\Delta E = 1.89$ eV, additional directions (11 and 12) are becoming active as well.

These simulations are useful for the identification of the types of products to be expected from the deactivation at the ring-opened conical intersection. The obtained fraction of non-cyclic structures, however, cannot be directly compared with the experimental number of fragments coming from ring-opening processes because in the simulations the initial velocities were isotropically generated. In the full dynamics simulation, the history of pyrrole derived from the dynamics on the excited state surface should create a bias towards some specific directions. This is an important point to be investigated in a future work.

8.7. CONCLUSIONS AND FINAL REMARKS

We have discussed how multireference ab inito molecular dynamics, although still very challenging, is becoming a useful tool for the investigation of photochemical processes in heterocycles. The dynamics of three particular molecules, aminopyrimidine, pyridone, and pyrrole has been discussed. Several aspects of the excited state reaction paths and conical intersections in heterocyclic systems have been reviewed as well. It has been argued that the well-known torsional conical intersections that appear in open π systems are closely related in terms of electronic structure to the puckered conical intersections appearing in 6-membered aromatic and heteroaromatic rings. In both cases, torsion and puckering, the conical intersections have their origin from the torsional relaxation of the biradical S_1 state. Besides that, we have also pointed out that the stretching-bipyramidalization motion – the other mode of biradical-state relaxation and closed-shell ground state destabilization – should play a similar role in 5-membered heterocycles.

One point of particular relevance in the photodynamics that has not been addressed is the effect of the environment (external fields, solvents, solid surfaces, and protein cavities). Environmental effects can change the relative position of the electronic states, the position, and the topology of the conical intersections [62]. It is still early to say whether it is possible to establish principles to make general predictions about the environmental effects on the photodynamics or it will be always necessary to make a particular analysis for each system. In

any case, the environmental influences on the nonadiabatic photodynamics have become a very active research area [62, 98–104] and certainly important contributions can be expected in the near future. In terms of CASSCF and MRCI ab initio dynamics simulations, work is in progress in our group on the implementation of QM/MM approaches that should allow the investigation of solvation effects for molecular systems of at least similar sizes as discussed here for gas phase.

ACKNOWLEDGEMENTS

This work has been supported by the Austrian Science Fund within the framework of the Special Research Program F16 (Advanced Light Sources) and Project P18411-N19. The authors are grateful for technical support and computer time at the Linux PC cluster Schrödinger III of the computer center of the University of Vienna.

REFERENCES

1. Canuel C, Mons M, Piuzzi F, Tardivel B, Dimicoli I, Elhanine M (2005) J Chem Phys 122: 074316.
2. Matsika S (2004) J Phys Chem A 108: 7584.
3. Shukla MK, Leszczynski J (2004) J Comput Chem 25: 768.
4. Blancafort L, Cohen B, Hare PM, Kohler B, Robb MA (2005) J Phys Chem A 109: 4431.
5. Chen H, Li SH (2005) J Phys Chem A 109: 8443.
6. Marian CM (2005) J Chem Phys 122: 104314.
7. Perun S, Sobolewski AL, Domcke W (2005) J Am Chem Soc 127: 6257.
8. Perun S, Sobolewski AL, Domcke W (2005) Chem Phys 313: 107.
9. Serrano-Andrés L, Merchán M, Borin AC (2006) Proc Natl Acad Sci U S A 103: 8691.
10. Marian CM (2007) J Phys Chem A 111: 1545.
11. Tully JC (1998) Faraday Discuss 110: 407.
12. Klein S, Bearpark MJ, Smith BR, Robb MA, Olivucci M, Bernardi F (1998) Chem Phys Lett 292: 259.
13. Weber W, Thiel W (2000) Theor Chem Acc 103: 495.
14. Strodel P, Tavan P (2002) J Chem Phys 117: 4667.
15. Ciminelli C, Granucci G, Persico M (2004) Chem Eur J 10: 2327.
16. Toniolo A, Olsen S, Manohar L, Martinez TJ (2004) Faraday Discuss 127: 149.
17. Bauernschmitt R, Ahlrichs R (1996) Chem Phys Lett 256: 454.
18. Bauernschmitt R, Haser M, Treutler O, Ahlrichs R (1997) Chem Phys Lett 264: 573.
19. Furche F, Ahlrichs R (2002) J Chem Phys 117: 7433.
20. Hättig C (2003) J Chem Phys 118: 7751.
21. Kohn A, Hättig C (2003) J Chem Phys 119: 5021.
22. Stanton JF, Bartlett RJ (1993) J Chem Phys 98: 7029.
23. Stanton JF, Gauss J (1994) J Chem Phys 100: 4695.
24. Grimme S, Waletzke M (1999) J Chem Phys 111: 5645.

25. Hirao K (1992) Chem Phys Lett 190: 374.
26. Nakano H (1993) J Chem Phys 99: 7983.
27. Kozlowski PM, Davidson ER (1994) J Chem Phys 100: 3672.
28. Roos BO, Andersson K, Fülscher MP, Malmqvist PA, Serrano-Andrés L, Pierloot K, Merchán M (1996) Adv Chem Phys 93: 219.
29. Celani P, Werner HJ (2003) J Chem Phys 119: 5044.
30. Shepard R, Lischka H, Szalay PG, Kovar T, Ernzerhof M (1992) J Chem Phys 96: 2085.
31. Bearpark MJ, Robb MA, Schlegel HB (1994) Chem Phys Lett 223: 269.
32. Lischka H, Dallos M, Shepard R (2002) Mol Phys 100: 1647.
33. Dallos M, Lischka H, Shepard R, Yarkony DR, Szalay PG (2004) J Chem Phys 120: 7330.
34. Lischka H, Dallos M, Szalay PG, Yarkony DR, Shepard R (2004) J Chem Phys 120: 7322.
35. Lischka H, Shepard R, Brown FB, Shavitt I (1981) Int J Quantum Chem S.15: 91.
36. Lischka H, Shepard R, Shavitt I, Pitzer RM, Dallos M, Mueller T, Szalay PG, Brown FB, Ahlrichs R, Boehm HJ, Chang A, Comeau DC, Gdanitz R, Dachsel H, Ehrhardt C, Ernzerhof M, Hoechtl P, Irle S, Kedziora G, Kovar T, Parasuk V, Pepper MJM, Scharf P, Schiffer H, Schindler M, Schueler M, Seth M, Stahlberg EA, Zhao J-G, Yabushita S, Zhang Z, Barbatti M, Matsika S, Schuurmann M, Yarkony DR, Brozell SR, Beck EV, Blaudeau J-P (2006) COLUMBUS: an ab initio electronic structure program, release 5.9.1: www.univie.ac.at/columbus.
37. Barbatti M, Granucci G, Lischka H, Ruckenbauer M, Persico M (2007) NEWTON-X: a package for Newtonian dynamics close to the crossing seam, version 0.13b: www.univie.ac.at/newtonx.
38. Barbatti M, Granucci G, Persico M, Ruckenbauer M, Vazdar M, Eckert-Maksic M, Lischka H (2007) J Photochem Photobio A 190: 228.
39. Swope WC, Andersen HC, Berens PH, Wilson KR (1982) J Chem Phys 76: 637.
40. Andersen HC (1980) J Chem Phys 72: 2384.
41. Tully JC (1990) J Chem Phys 93: 1061.
42. Hammes-Schiffer S, Tully JC (1994) J Chem Phys 101: 4657.
43. Granucci G, Persico M (2007) J Chem Phys 126: 134114.
44. Lischka H, Shepard R, Pitzer RM, Shavitt I, Dallos M, Muller T, Szalay PG, Seth M, Kedziora GS, Yabushita S, Zhang ZY (2001) PCCP 3: 664.
45. Ahlrichs R, Bär M, Häser M, Horn H, Kölmel C (1989) Chem Phys Lett 162: 165.
46. Stanton JF, Gauss J, Watts JD, Lauderdale WJ, Bartlett RJ (1992) Int J Quantum Chem S 26: 879.
47. Bunge A (1970) J Chem Phys 53: 20.
48. Langhoff SR, Davidson ER (1974) Int J Quantum Chem 8: 61.
49. Bruna PJ, Peyerimhoff SD, Buenker RJ (1980) Chem Phys Lett 72: 278.
50. Shepard R (1995) In: Yarkony DR (ed) Modern Electronic Structure Theory (Advanced Series in Physical Chemistry), vol. 1. World Scientific: Singapore, p. 345.
51. Hehre WJ, Ditchfie.R, Pople JA (1972) J Chem Phys 56: 2257.
52. Binkley JS, Pople JA, Hehre WJ (1980) J Am Chem Soc 102: 939.
53. Butcher J (1965) J Assoc Comput Mach 12: 124.
54. Hill AD, Reilly PJ (2007) J Chem Inf Model 47: 1031.
55. Cremer D, Pople JA (1975) J Am Chem Soc 97: 1354.
56. Cremer D (1984) Acta Crystallogr, Sect B: Struct Sci 40: 498.
57. Boeyens JCA (1978) J Chem Crystallogr 8: 317.
58. Evans DG, Boeyens JCA (1989) Acta Crystallogr, Sect B: Struct Sci 45: 581.
59. Spek AL (2003) J Appl Crystallogr 36: 7.
60. Bonačić-Koutecký V, Koutecký J, Michl J (1987) Angew Chem Int Ed Engl 26: 170.
61. Martinez TJ (2006) Acc Chem Res 39: 119.

62. Burghardt I, Hynes JT (2006) J Phys Chem A 110: 11411.
63. Ohmine I (1985) J Chem Phys 83: 2348.
64. Michl J, Bonačić-Koutecký V (1990) Electronic Aspects of Organic Photochemistry, Wiley-Interscience, New york.
65. Barbatti M, Paier J, Lischka H (2004) J Chem Phys 121: 11614.
66. Zechmann G, Barbatti M, Lischka H, Pittner J, Bonačić-Koutecký V (2006) Chem Phys Lett 418: 377.
67. Barbatti M, Lischka H (2007) J Phys Chem A 111: 2852.
68. Barbatti M, Vazdar M, Aquino AJA, Eckert-Maksic M, Lischka H (2006) J Chem Phys 125: 164323.
69. Wilsey S, Houk KN (2002) J Am Chem Soc 124: 11182.
70. Barbatti M, Aquino AJA, Lischka H (2005) J Phys Chem A 109: 5168.
71. Barbatti M, Rocha AB, Bielschowsky CE (2005) Phys Rev A 72: 0232711.
72. Sobolewski AL, Woywod C, Domcke W (1993) J Chem Phys 98: 5627.
73. Garavelli M, Page CS, Celani P, Olivucci M, Schmid WE, Trushin SA, Fuss W (2001) J Phys Chem A 105: 4458.
74. Bearpark MJ, Bernardi F, Clifford S, Olivucci M, Robb MA, Vreven T (1997) J Phys Chem A 101: 3841.
75. Su MD (2006) J Phys Chem A 110: 9420.
76. Perun S, Sobolewski AL, Domcke W (2006) J Phys Chem A 110: 13238.
77. Ismail N, Blancafort L, Olivucci M, Kohler B, Robb MA (2002) J Am Chem Soc 124: 6818.
78. Frey JA, Leist R, Tanner C, Frey HM, Leutwyler S (2006) J Chem Phys 125: 114308.
79. Amatatsu Y, Komura Y (2006) J Chem Phys 125: 174311.
80. Garavelli M, Bernardi F, Cembran A, Castano O, Frutos LM, Merchan M, Olivucci M (2002) J Am Chem Soc 124: 13770.
81. Meuwly M, Müller A, Leutwyler S (2003) Phys Chem Chem Phys 5: 2663.
82. Frey JA, Leist R, Müller A, Leutwyler S (2006) ChemPhysChem 7: 1494.
83. Barbatti M, Aquino AJA, Lischka H (2008) Chem Phys: doi: 10.1016/j.chemphys.2008.02.007
84. Sobolewski AL, Domcke W, Dedonder-Lardeux C, Jouvet C (2002) Phys Chem Chem Phys 4: 1093.
85. Wei J, Riedel J, Kuczmann A, Renth F, Temps F (2004) Faraday Discuss 127: 267.
86. Zgierski MZ, Patchkovskii S, Fujiwara T, Lim EC (2005) J Phys Chem A 109: 9384.
87. Bernardi F, Olivucci M, Robb MA (1996) Chem Soc Rev 25: 321.
88. Palmer IJ, Olivucci M, Bernardi F, Robb MA (1992) J Org Chem 57: 5081.
89. Bearpark MJ, Boggio-Pasqua M, Robb MA, Ogliaro F (2006) Theor Chem Acc 116: 670.
90. Barbatti M, Aquino AJA, Lischka H (2006) Mol Phys 104: 1053.
91. Salzmann S, Kleinschmidt M, Tatchen J, Weinkauf R, Marian CM (2008) Phys Chem Chem Phys 10: 380.
92. Migani A, Gentili PL, Negri F, Olivucci M, Romani A, Favaro G, Becker RS (2005) J Phys Chem A 109: 8684.
93. Fuss W, Hofer T, Hering P, Kompa KL, Lochbrunner S, Schikarski T, Schmid WE (1996) J Phys Chem 100: 921.
94. Barbatti M, Ruckenbauer M, Szymczak JJ, Aquino AJA, Lischka H (2008) Phys Chem Chem Phys 10: 482.
95. Crespo-Hernández CE, Cohen B, Hare PM, Kohler B (2004) Chem Rev 104: 1977.
96. Atchity GJ, Xantheas SS, Ruedenberg K (1991) J Chem Phys 95: 1862.
97. Migani A, Olivucci M (2004) Conical Intersections: Electronic Structure, Dynamics & Spectroscopy. World Scientific Publishing Company.

98. Burghardt I, Cederbaum LS, Hynes JT (2004) Faraday Discuss 127: 395.
99. Cembran A, Bernardi F, Olivucci M, Garavelli M (2004) J Am Chem Soc 126: 16018.
100. Langer H, Doltsinis NL, Marx D (2005) Chem Phys Chem 6: 1734.
101. Yamazaki S, Kato S (2005) J Chem Phys 123: 114510.
102. Mercier SR, Boyarkin OV, Kamariotis A, Guglielmi M, Tavernelli I, Cascella M, Rothlisberger U, Rizzo TR (2006) J Am Chem Soc 128: 16938.
103. Spezia R, Burghardt I, Hynes JT (2006) Mol Phys 104: 903.
104. Santoro F, Barone V, Gustavsson T, Improta R (2006) J Am Chem Soc 128: 16312.